Journal of Wind Engineering & Industrial Aerodynamics 177 (2018) 293–305

Contents lists available at ScienceDirect

Journal of Wind Engineering & Industrial Aerodynamics

journal homepage: www.elsevier.com/locate/jweia

Numerical study of turbulent flow fields around of a row of trees and an isolated building by using modified k-ε model and LES model

Yihong Qi *, Takeshi Ishihara

Department of Civil Engineering, School of Engineering, The University of Tokyo, Tokyo, Japan

ARTICLE INFO

Keywords:
Turbulent flow fields over urban elements
Modified $k-\varepsilon$ model
LES model
Validation metrics
Vortex cores
Quadrant analysis

ABSTRACT

Turbulent flow fields over two typical urban elements, a row of trees with low packing density and an isolated building with high packing density, are investigated by a modified $k-\varepsilon$ model and a LES model. The applicability of these two models is evaluated by the validation metrics. Instantaneous flow fields are visualized by vortex cores and examined by quadrant analysis. In the wake region of the row of trees, predicted mean wind speed by the modified $k-\varepsilon$ model shows favourable agreement with the measured data, but turbulent kinetic energy is underestimated since the modified $k-\varepsilon$ model is not capable of simulating organized motions. In the wake region of the isolated building, both predicted mean wind speed and turbulent kinetic energy by the modified $k-\varepsilon$ model are slightly underestimated due to lack of the vortex shedding in the simulation. On the other hand, LES model well predicts both mean wind speed and turbulent kinetic energy since all large vortices are directly resolved by LES model.

1. Introduction

With increasing requirement on renewable energy, wind turbines are installed in or near the urban and suburban areas, where the local wind condition is strongly affected by surrounding trees and buildings. Prediction of mean wind speed and turbulence are important, because mean wind speed is directly related to potential wind energy, while turbulence results in fluctuating wind load on the structure components and affects the fatigue life of wind turbine. Therefore, accurate prediction of turbulent flow fields around trees and buildings is necessary not only for designing of wind turbine but also for maintenance of wind turbines (IEC 61400-2, 2006).

With the aim of providing accurate prediction of turbulent flow field in the urban area, modelling of the effect of surface roughness is a key factor. Surface roughness trees and buildings are dominant and modelling them is necessary. As to modelling buildings, the rigid wall approach was applied by many researches (Gousseau et al. (2011), Blocken et al. (2012), Philips et al. (2013) and Cheng and Porte-Agel (Cheng and Porté-Agel, 2015), Mochida et al. (2002), Tominaga et al. (2008) and Gousseau et al. (2013)), in which detailed geometry information of each building are used and wall functions are applied for the boundary condition of building surface. However, this approach requires large effort on grid generation and calculation, and its application is therefore limited to a small area. On modelling vegetation, the canopy model is the only choice, which considers the fluid force and, turbulence generation and dissipation due to obstacles by introducing source terms into the momentum equation and turbulence transportation equations. Researches on canopy model with Reynolds average turbulence model (RANS) for vegetation and unban canopies have been carried out by Wilson (1988), Green (1992), Liu et al. (1996), Aumond et al. (2013), Suzuki et al. (2002) and Iwata et al. (2004), Maruyama (1993), Salim et al. (2015). However, conventional canopy models have a limitation that they can only be applicable to the canopy with a low packing density. Moreover, Mochida et al. (2008) provided a detailed comparison of various RANS models for the simulation of the wind flow through the row of trees, but the organized motions around them and the reason of discrepancies between predicted and measured turbulent flow fields should be further demonstrated. Enoki et al. (2009) and Enoki and Ishihara (2012) proposed a generalized canopy model which is able to consider the effect of the vegetation and buildings simultaneously. The generalized canopy model together with a modified $k-\varepsilon$ model has been applied for wind prediction of a single building as well as a real urban area. Comparing with rigid wall approach, the canopy model relax the requirement of geometry in the region close to obstacles, and it allows less computational grid. Furthermore, a simple grid system can be used in any size of urban areas. However, there are still some discrepancies

* Corresponding author.
E-mail address: qi@bridge.t.u-tokyo.ac.jp (Y. Qi).

https://doi.org/10.1016/j.jweia.2018.04.007
Received 12 July 2017; Received in revised form 1 October 2017; Accepted 9 April 2018

between predicted and measured flow field and the reasons should be investigated. Moreover, accuracy of the LES model with the generalized canopy model has not been evaluated yet.

LES models are also used with rigid wall approach to predict unsteady flow fields over buildings (Rodi (1997), Yoshie et al., 2007, 2011 and Xie and Castro (2006)). They attributed the good performance of LES model to predict periodic vortex shedding and highlighted the importance of inflow turbulence on the accuracy of simulation using LES model. On modelling trees, some efforts were also made by using LES model (Yang et al. (2006), Bailey and Stoll (2013), Mueller et al. (2014) and Lopes et al. (2013)). However, accurate prediction with LES model depends on several issues, such as turbulent inflow condition and grid resolution. Therefore, a comparison between RANS and LES models for canopy flows with low and high packing densities is necessary to clarify the applicability of each turbulence model.

In this study, the numerical methods are given in section 2, including governing equations, fluid force and turbulence models, boundary condition and numerical schemes used in the simulations, as well as analysis methods applied in the discussion. In section 3, two typical urban elements are discussed. At first, the experiment in each case is briefly described, then turbulent flow fields are investigated and applicability of these two models is evaluated by the validation metrics. Instantaneous flow fields are visualized by vortex cores and examined by the quadrant analysis. Finally, conclusions are shown in section 4 based on above discussions.

2. Numerical method

2.1. Governing equations

For the analysis of the flow field with obstacles inside, two different approaches are used. The governing equations are constructed for the fluid part only in one approach, and for the flow field averaged over the computational grid in the other approach. In this study, the latter approach is used. The averaged continuity and momentum equations for incompressible flow with considering the effect of the buildings and vegetation are given by:

$$\frac{\partial(\rho\overline{u}_i)}{\partial x_i} = 0 \tag{1}$$

$$\frac{\partial(\rho\overline{u}_i)}{\partial t} + \frac{\partial(\rho\overline{u}_j\overline{u}_i)}{\partial x_j} = -\frac{\partial\overline{p}}{\partial x_i} + \frac{\partial}{\partial x_j}\left[\mu\left(\frac{\partial\overline{u}_i}{\partial x_j} + \frac{\partial\overline{u}_j}{\partial x_i}\right)\right] + \frac{\partial\tau_{ij}}{\partial x_j} + f_{\overline{u},i} \tag{2}$$

where $\overline{u}_i$ is the wind velocity in the ith direction ($u_1 = u$, $u_2 = v$ *and* $u_3 = w$). $\overline{p}$ is pressure, ρ is density of the fluid, μ is the molecular viscosity and $f_{\overline{u},i}$ is the fluid force per unit grid volume due to obstacles which is described in section 2.2. The overbar indicates time averaged mean value in the simulation with the modified $k-\varepsilon$ model, while it indicates the resolved value in the simulation with LES model. τ_{ij} is introduced to consider difference between $\overline{u_i u_j}$ and $\overline{u}_i\overline{u}_j$, i.e.,

$$\tau_{ij} = -\rho\left(\overline{u_i u_j} - \overline{u}_i\overline{u}_j\right) \tag{3}$$

Although the expression of τ_{ij} in Eq. (3) is the same for the modified $k-\varepsilon$ model and the LES model, its meaning is different in the two models. τ_{ij} in the modified $k-\varepsilon$ model is time-averaged Reynolds stress and stands for effect from vortex to mean flow field, while τ_{ij} in LES indicates the subgrid-scale Reynolds stress and accounts for contribution from unresolved smaller vortex to large size vortex.

2.2. Fuid force model

The generalized canopy model derived by Enoki and Ishihara (2012) is applied in this study and the fluid force in the momentum equations is:

Table 1
Parameters in the conventional and the generalized canopy models.

Type of obstacles	Conventional canopy model	Generalized canopy model
Vegetation (Wilson, 1988)	$f_{\overline{u},i} = -\frac{1}{2}\rho C_{D,t} a_t \lvert\overline{u}\rvert\overline{u}_i$	$C_f = C_{D,t}$ $\gamma_0 = a_t l_0$ $l_0 = 10^{-3}(m)$
Buildings (Maruyama, 1993)	$f_{\overline{u},i} = -\frac{1}{2}\rho C_{D,b} a_b \lvert\overline{u}\rvert\overline{u}_i$ $\gamma_b = V_b/V_{grid}$ $a_b = \frac{S_b}{4(1-\gamma_b)V_{grid}}$	$C_f = C_{D,b}/(1-\gamma_b)^3 = \frac{1}{(1-\gamma_b)^3} min\left[\frac{1.53}{1-\gamma_b}, 2.75(1-\gamma_b)\right]$ $\gamma_0 = \gamma_b$ $l_0 = 4V_b/S_b\ (m)$

$$f_{\overline{u},i} = -\frac{F_{\overline{u},i}}{V_{grid}} = -\frac{1}{2}\rho C_f \frac{\gamma_0}{l_0}\lvert\overline{u}\rvert\overline{u}_i \tag{4}$$

where, $f_{\overline{u},i}$ is the fluid force in the volume of grid, V_{grid}. $\lvert\overline{u}\rvert$ is the absolute value of mean wind speed per unit volume, C_f is the equivalent drag coefficient, l_0 is defined as the representative length scale of obstacles and γ_0 is the packing density. Canopy parameters for vegetation and buildings are summarized in Table 1, where $C_{D,t}$ and a_t are the drag coefficient and the leaf area density of vegetation respectively, $C_{D,b}$, V_b and S_b are the drag coefficient, the total volume and the total side surface of buildings.

2.3. Turbulence model

For the closure of the governing equations, τ_{ij} has to be modelled. In the modified $k-\varepsilon$ model, τ_{ij} is approximated by the linear turbulence viscosity model, i.e.,

$$\tau_{ij} = -\rho\overline{u'_i u'_j} = 2\mu_t\overline{S}_{ij} - \frac{2}{3}\rho k\delta_{ij} \tag{5}$$

where δ_{ij} is the Kronecker delta. Turbulence viscosity μ_t and rate-of-strain tensor $\overline{S}_{ij}$ are expressed as:

$$\mu_t = C_\mu\rho\frac{\overline{k}^2}{\overline{\varepsilon}} \tag{6}$$

$$\overline{S}_{ij} = \frac{1}{2}\left(\frac{\partial\overline{u}_i}{\partial x_j} + \frac{\partial\overline{u}_j}{\partial x_i}\right) \tag{7}$$

In the modified $k-\varepsilon$ model, two additional equations are used to calculate the turbulent kinetic energy, k, and the dissipation rate, ε.

$$\frac{\partial\rho\overline{k}}{\partial t} + \frac{\partial\rho\overline{u}_j\overline{k}}{\partial x_j} = \frac{\partial}{\partial x_j}\left[\left(\mu + \frac{\mu_t}{\sigma_k}\right)\frac{\partial\overline{k}}{\partial x_j}\right] - \left[\frac{2}{3}\rho\overline{k}\delta_{ij}\frac{\partial\overline{u}_i}{\partial x_j} - P_k\right] - \rho\overline{\varepsilon} + f_k \tag{8}$$

$$\frac{\partial\rho\overline{\varepsilon}}{\partial t} + \frac{\partial\rho\overline{u}_j\overline{\varepsilon}}{\partial x_j} = \frac{\partial}{\partial x_j}\left[\left(\mu + \frac{\mu_t}{\sigma_\varepsilon}\right)\frac{\partial\overline{\varepsilon}}{\partial x_j}\right] - C_{\varepsilon 1}\frac{\overline{\varepsilon}}{\overline{k}}\left[\frac{2}{3}\rho\overline{k}\delta_{ij}\frac{\partial\overline{u}_i}{\partial x_j} - P_k\right] - C_{\varepsilon 2}\frac{\rho\overline{\varepsilon}^2}{\overline{k}} + f_\varepsilon \tag{9}$$

Parameters in the above equations are the same as those used in the standard $k-\varepsilon$ model, i.e., $C_\mu = 0.09$, $\sigma_k = 1.0$, $C_\varepsilon = 1.3$, $C_{\varepsilon 1} = 1.44$ and $C_{\varepsilon 2} = 1.92$. In order to settle overestimation of turbulent kinetic energy at stagnation point, turbulence source term P_k is estimated by Kato and Launder model (Kato, 1993). The source terms for turbulent kinetic energy and its dissipation rate are introduced to consider the promoting process of energy cascade in canopy layer. The model proposed by Enoki and Ishihara (Enoki et al., 2009; Enoki and Ishihara, 2012) is adopted and can be expressed as:

$$f_k = \frac{1}{2}\beta_p\rho C_f a\left|\overline{u}\right|^3 - \frac{1}{2}\beta_d\rho C_f a\left|\overline{u}\right|\overline{k} \tag{10}$$

$$f_\varepsilon = \frac{1}{2}C_{p\varepsilon 1}\beta_p\rho\frac{\overline{\varepsilon}}{\overline{k}}C_f a|\overline{u}|^3 - \frac{1}{2}C_{p\varepsilon 2}\beta_d\rho C_f a|\overline{u}|\overline{\varepsilon} \tag{11}$$

where the model constants β_p and $C_{p\varepsilon 1}$ are set to 1.0 and 1.5 respectively. β_d and $C_{p\varepsilon 2}$ are modelled as the functions of the packing density γ_0. The generation and dissipation of turbulence are assumed to be cancelled out in high packing density region and then β_d and $C_{p\varepsilon 2}$ can be obtained from:

$$\beta_d = \min\left[4.0, \alpha_{k1}\exp\left(\frac{1-\gamma_0}{\gamma_0}\right) + \alpha_{k2}\right] \tag{12}$$

$$C_{p\varepsilon 2} = \begin{cases} 0.7 & ,\gamma_0 \le \gamma_c \\ \alpha_{\varepsilon 1}\sqrt{\sin\left(\pi\frac{\gamma_0-\gamma_c}{2(1-\gamma_c)}\right)} + \alpha_{\varepsilon 2} & ,\gamma_0 > \gamma_c \end{cases} \tag{13}$$

where the coefficients are identified to be $\alpha_{k1} = 0.5$, $\alpha_{k2} = 0.5$, $\alpha_{\varepsilon 1} = 0.8$, $\alpha_{\varepsilon 2} = 0.7$ and $\gamma_c = 0.312$.

In LES model, the subgrid-scale Reynolds stress τ_{ij} is modelled as:

$$\tau_{ij} = -2\mu_t\overline{S}_{ij} + \frac{1}{3}\tau_{kk}\delta_{ij} \tag{14}$$

where, μ_t denotes subgrid-scale turbulent viscosity and modelled by Smagorinsky-Lilly model, and $\overline{S}_{ij}$ is the rate-of-strain tensor for the resolved scale.

$$\mu_t = \rho L_s^2|\overline{S}| = \rho L_s^2\sqrt{2\overline{S}_{ij}\overline{S}_{ij}} \tag{15}$$

where L_s is the mixing length for subgrid-scales, and defined as:

$$L_s = \min\left(\kappa d, C_s V^{\frac{1}{3}}\right) \tag{16}$$

where $\kappa = 0.42$ is the von Karman constant. d is the distance to the closest wall and V is the volume of a computational grid. C_s is Smagorinsky constant and in this study $C_s = 0.032$ is chosen based on Oka and Ishihara (2009).

In the case of the modified $k-\varepsilon$ model is used, additional parameters are introduced in k and ε equations to model turbulence generated and dissipated by the canopy. On the other hand, LES model directly resovles turbulence generated and dissipated in the canopy region and doesn't introduce any new parameters.

2.4. Boundary condition and solution scheme

Boundary conditions and numerical schemes used in simulations with the modified $k-\varepsilon$ model and LES model are summarized in Table 2 and Table 3. The inlet and bottom boundary conditions for LES model are much difficult than those for the modified $k-\varepsilon$ model. A numerical wind tunnel concept is used in this study to generate turbulent inflow for LES model, in which the same vortex generators, such as spires, fences and blocks, are used as those in the wind tunnel test. On the other hand, the measured mean wind speed and turbulence profiles are directly used for the modified $k-\varepsilon$ model as mentioned in Section 3.

The steady simulation is conducted with the modified $k-\varepsilon$ model. The measured wind speed and turbulent kinetic energy are directly used for the inlet boundary. On the other hand, the unsteady simulation is conducted with the LES model. Statistical values of wind speed and turbulent kinetic energy are calculated and compared with the measured data. A non-dimensional time step $\Delta tU_{ref}/H = 0.005$ is used for both cases in this study. The averaged wind speed is obtained by calculating the time average over a non-dimensional time tU_{ref}/H from 200 to 800. The turbulent kinetic energy is calculated as $TKE = 0.5\times[\sigma_u^2+\sigma_v^2+\sigma_w^2]$. A stationary condition can be achieved by evaluating relative errors of streamwise mean wind speed and turbulent kinetic energy at selected point in the wake region (x/H = 3, y/H = 0, z/H = 0.643 for the row of tree; x/H = 1, y/H = 0, z/H = 0.5 for the isolated building). The first 200 non-dimensional time data are removed to eliminate the transit data. For the non-dimensional time period of 600, the relative error of streamwise mean wind speed is less than 1% and the turbulent kinetic energy is less than 3% for all cases of LES simulations.

Table 2
Boundary conditions.

	modified $k-\varepsilon$	LES
Outlet Boundary	Outflow	Outflow
Side Boundary	Symmetry	Symmetry
Top Boundary	Symmetry	Symmetry

Table 3
Numerical schemes.

	modified $k-\varepsilon$	LES
Turbulence Model	modified $k-\varepsilon$ model	Smagorinsky-Lilly model
Spatial discretization method	QUICK	CDS
Time discretization method	–	2nd order implicit scheme
Pressure-velocity coupling	SIMPLE	SIMPLE

2.5. Validation metrics and analysis methods

In order to quantify the agreement between computational and experimental results, validation metrics, including the hit rate q and the fraction of the prediction within a factor of 2 of the observation, FAC2, were used (Schatzmann et al., 2010). The definition of q and FAC2 are given in Eqs. (17) and (18), respectively and the boundaries of accurate region are shown schematically in Fig. 1.

$$q = \frac{1}{N}\sum_{i=1}^{N} n_i within_i = \begin{cases} 1 & \left|\frac{y_i - x_i}{x_i}\right| \le D_q or |y_i - x_i| \le W_q \\ 0 & else \end{cases} \tag{17}$$

$$FAC2 = \frac{1}{N}\sum_{i=1}^{N} n_i within_i = \begin{cases} 1 & 0.5 \le \frac{y_i}{x_i} \le 2 \\ 0 & else \end{cases} \tag{18}$$

In these definitions, x_i and y_i are the obvserved (measured) and predicted (computed) values of a given variable for smaple i, respectively, and N is the number of data points. The ideal values of the metrics that correspond to perfect agreement are 1.0 for q and FAC2. The

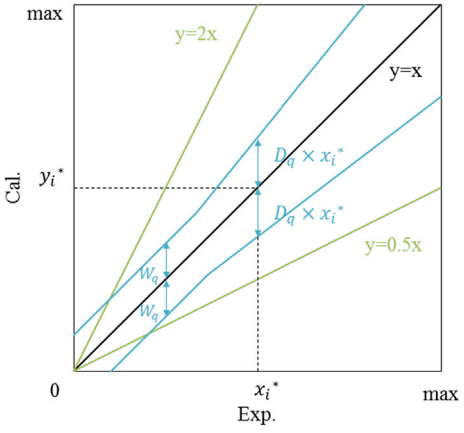

Fig. 1. Validation Metrics. The lines in blue and green mark the boundaries defined by q and FAC2, respectively. (For interpretation of the references to colour in this figure legend, the reader is referred to the Web version of this article.)

thresholds for q are $D_q = 0.15$ for mean wind speed and $D_q = 0.3$ for turbulent kinetic energy since the squared variable gives error as twice as the variable itself. $W_q = 0.05|\max|$ is used for both mean wind speed and turbulent kinetic energy, in which $|\max|$ is a maximum value supposed in the obvservation and the prediction as shown in Fig. 1.

Vorticity defined as Eq. (19), is usually used to identify vortices. However, as mentioned by Kida and Miura (1998), solely vorticity cannot distinguish between swirling and shearing motions. The λ_2-criterion proposed by Jeong and Hussaion (Jeong and Hussain, 1995) is used in this study, which searches a local pressure minimum due to vortical motions. It defines a vortex core as a connected region with two negative eigenvalues of system defined by Eq. (20), in which $\overline{S}_{ij}$ is the rate-of-strain tensor shown in Eq. (7) and $\overline{\Omega}_{ij}$ is the vorticity tensor defined in Eq. (21). This definition equals the requirement that λ_2 is negative when three eigenvalues are ordered as $\lambda_1 \geq \lambda_2 \geq \lambda_3$.

$$\omega_{ij} = \frac{\partial \overline{u}_i}{\partial x_j} - \frac{\partial \overline{u}_j}{\partial x_i} \tag{19}$$

$$\overline{S}_{ik}\overline{S}_{kj} + \overline{\Omega}_{ik}\overline{\Omega}_{kj} = 0 \tag{20}$$

$$\overline{\Omega}_{ij} = \frac{1}{2}\left(\frac{\partial \overline{u}_i}{\partial x_j} - \frac{\partial \overline{u}_j}{\partial x_i}\right) \tag{21}$$

In this study, the quadrant analysis is also applied for the quantitative evaluation of organized motions as shown by Oikawa and Meng (1995). Four quadrants of the Reynolds stresses are defined in Eq. (22). The quadrant analysis of $S_n(uv)$ and $S_n(uw)$ are widely used to clarify organized motions in the vertical and horizontal cross sections, respectively. The quadrants $S_2(uw)$ and $S_4(uw)$ represent ejection and sweep motions respectively and make positive contributions to the Reynolds stress, while quadrants $S_1(uw)$ and $S_3(uw)$ express outward and inward motions respectively and make negative contributions to the Reynolds stress. The difference, ΔS, between S_4 and S_2 indicates the intensity of organized motions. When the turbulent flow is fully developed and proceeds in a random way, the value of ΔS is close to zero, while it is not zero when the organized motions appear.

$$S_n(uw) = \begin{cases} -\overline{uw} & for\ (u > 0, w > 0)\ if\ n = 1 \\ -\overline{uw} & for\ (u < 0, w > 0)\ if\ n = 2 \\ -\overline{uw} & for\ (u < 0, w < 0)\ if\ n = 3 \\ -\overline{uw} & for\ (u > 0, w < 0)\ if\ n = 4 \end{cases} \tag{22}$$

3. Numerical results and discussion

In this section, two typical urban elements are discussed. Firstly, each case is briefly described, then turbulent flow fields are investigated and applicability of these two models is evaluated by using the validation metrics. Finally, instantaneous flow fields are visualized by vortex cores and examined by the quadrant analysis.

3.1. Turbulent flow field over a row of trees

The field measurement conducted by Kurotani et al. (2001) is selected for numerical simulations. The turbulent field for a row of trees in Izumo, Japan, was measured in detail to investigate windbreak effect. The thickness, length and height the row of trees is 2 m, 74 m and 7 m respectively. Field measurements were conducted at the same place twice with different covering ratios of leaves. The second field measurement with covering ratio of 81% is used in this study. The mean wind speed and turbulence were measured at 35 m upstream from the front of the row of trees and at the heights of 1 m, 3 m and 9 m. The wind direction was almost normal to the row of trees. The mean wind speed and turbulence in the region behind trees were measured at the locations of 7 m, 14 m, 21 m, 28 m and 35 m downstream of the row of trees at the heights of 1.5 m, 3 m, 4.5 m and 6 m. The trees were covered by the leaves from 1.2 m to 7 m. The layout of the row of trees in the vertical cross section and the locations of measurement are shown in Fig. 2.

For the simulation with the modified $k-\varepsilon$ model, both simulations with real scale trees and scaled trees are conducted. It is found that the Reynolds number effect is weak, so the simulation with a ratio of 1:100 is used in this study. The computational domain L_x, L_y and L_z are1.1 m, 1 m and 1.1 m, respectively. For the LES simulation, the row of trees is scaled down with a ratio of 1:100. The length, width and height of computational domain are 13.5 m, 1.8 m and 1.5 m, respectively. Three spires and a fence are used to generate turbulent inflow profiles as shown in Fig. 3. A canopy layer with the height of 0.026 m is introduced to adjust the mean wind speed profiles at the low elevation. The canopy parameters are set as $C_f\gamma_0/l_0 = 60$, which corresponds to the same effects as a staggered cubic array with a packing density $\gamma_0 = 29\%$.

A structural grid system is used in simulation with the modified $k-\varepsilon$ model, and 39 × 54 × 20 grid nodes is used in the streamwise, lateral and vertical directions, respectively. An uniform grid with resolution of 0.02 m is used in the lateral direction, and a non-uniform grid is adopted in the streamwise and vertical directions. The minimum grid resolutions in the streamwise and vertical directions are 0.01 m and 0.005 m, respectively. In LES simulation, a structural grid system is also used in the region around the row of trees, while an un-structural grid is used around spires and fence. In the region around the row of trees, the minimum grid resolutions in the streamwise, lateral and vertical directions are 0.002 m, 0.005 m and 0.00025 m, respectively. Grid dependency is checked for both simulations by using twice finer grid around the row of trees. The same profiles are obtained, indicating the present grid is fine enough.

Boundary conditions at outlet, side and top of computational domain for the simulations with the modified $k-\varepsilon$ model and the LES model are summarized in Table 2. In the simulation with the modified $k-\varepsilon$ model, $z_0 = 1 \times 10^{-4} m$ is used for the ground surface. The measured mean wind speed and turbulence are used at the inlet boundary. In the simulation with LES model, uniform wind speed of 10 m/s is set at the inlet boundary as shown in Fig. 3(a). The canopy parameters are the same as those used by Enoki and Ishihara (2012). The packing density, γ_0, is 1.17×10^{-3}, and the representative length scale, l_0, is 1×10^{-3}m, in real scale, which correspond to $a_t = 1.17\mathrm{m}^{-1}$ in the conventional fluid force model for vegetation. The equivalent drag coefficient is $C_f = 1.6$. The representative length scale is also scaled down with a ratio of 1:100.

The predicted and measured profiles of mean wind speed and turbulent kinetic energy at the location P_0 are shown in Fig. 4. The turbulent

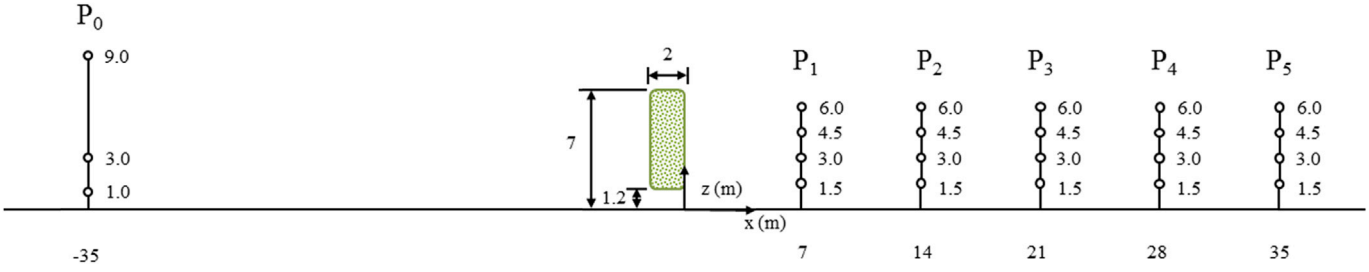

Fig. 2. Layout and measurement positions in the field measurement of a row of trees.

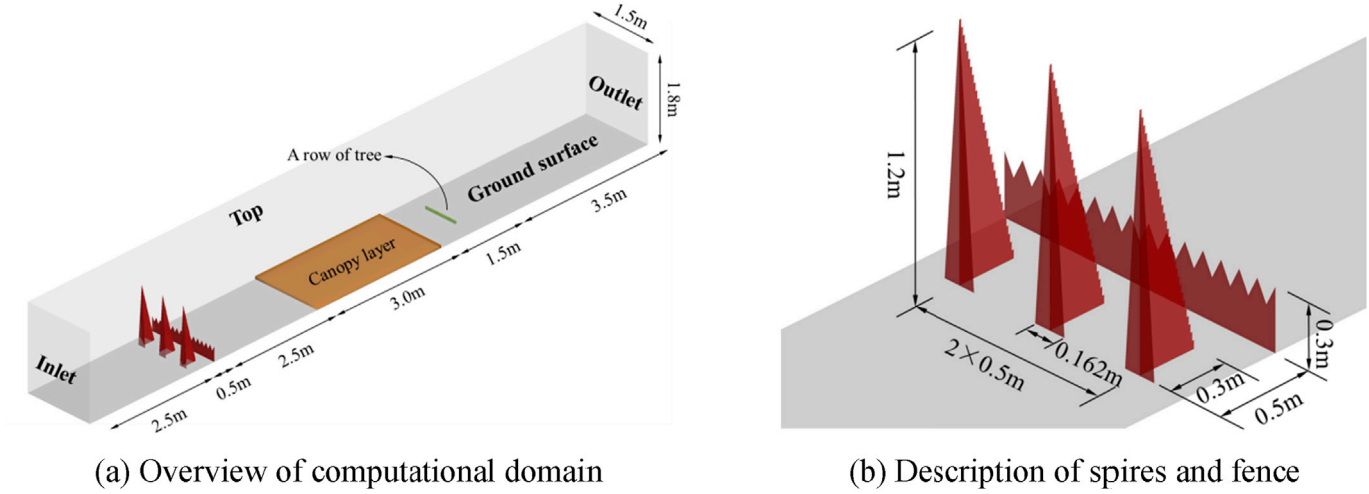

Fig. 3. Configuration of the numerical simulation of a row of trees with LES model.

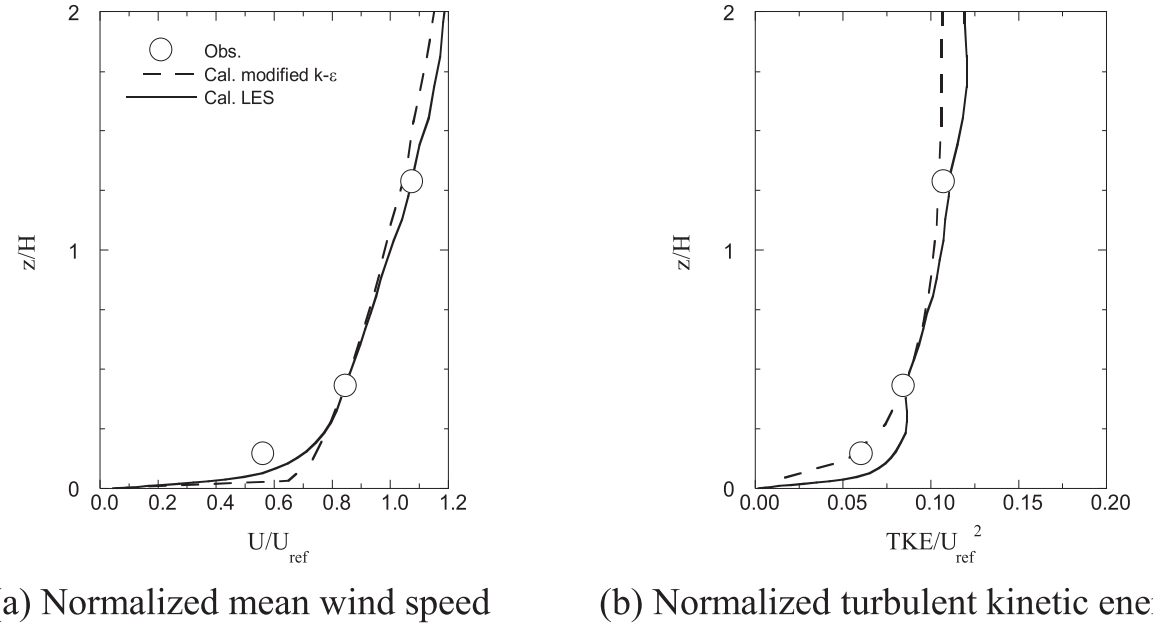

Fig. 4. Predicted and measured profiles of mean wind speed and turbulent kinetic energy at the location P0 for the case of a row of trees.

wind flow at the front of the row of trees has been favourably reproduced by the modified $k-\varepsilon$ model and LES model.

The mean wind speed profiles, as shown in Fig. 5 (a), are normalized by U_{ref}, which is the mean wind speed at z/H = 1 and x/H = −5. H is the height of the row of trees. It is found that the predicted mean wind speed by the modified $k-\varepsilon$ model and LES model show good agreement with the measured data. The fluid forces model are the same in both models, thus it provides the same momentum loss in both simulations. This might be a reason why both simulations show good agreement with the measured mean wind speed. The speedup at the top and bottom of the trees are simulated well and becomes weak at the downstream locations. Moreover, the mean wind speeds in the near wake region are almost constant, which imply the turbulence in this region cannot be generated by the wind shear.

The normalized turbulent kinetic energy profiles in the wake region of trees are shown in Fig. 5 (b). It is found that the predicted turbulent kinetic energy by the modified $k-\varepsilon$ model in the wake region of trees is significantly underestimated. On the other hand, the predicted turbulent kinetic energy profiles by LES model show good agreement with the measured data. One possible reason is that the modified $k-\varepsilon$ model does not generate the turbulence in the region without the wind shear as discussed above.

Scatter plots of numerical results against experimental data are shown in Fig. 6. The validation metrics are summarized in Table 4. The FAC2 does not show the difference between the predicted mean wind speeds by the modified $k-\varepsilon$ model and LES model, but it is close to zero for the predicted turbulent kinetic energy by using the modified $k-\varepsilon$. q is a more strict criteria and present how much the LES model performs better than the modified $k-\varepsilon$ model for both mean wind speed and turbulence.

The contours of normalized mean wind speed and the streamlines in the vertical cross section from the simulation with LES model are shown in Fig. 7 (a). The dashed rectangular block marks the region occupied by trees. The contours of turbulent kinetic energy in the vertical cross section from the simulation with LES model are shown in Fig. 7 (b), and the size of near wake region is identified as about 3H.

The instantaneous flow field is investigated by vortex cores to clarify the organized motions in the wake of the row of trees. The iso-surface of λ_2 is used to represents the vortices generated by the trees as shown in Fig. 8. The block in light blue marks the canopy region occupied by trees and the iso-surface in green represents vortex cores with a value of

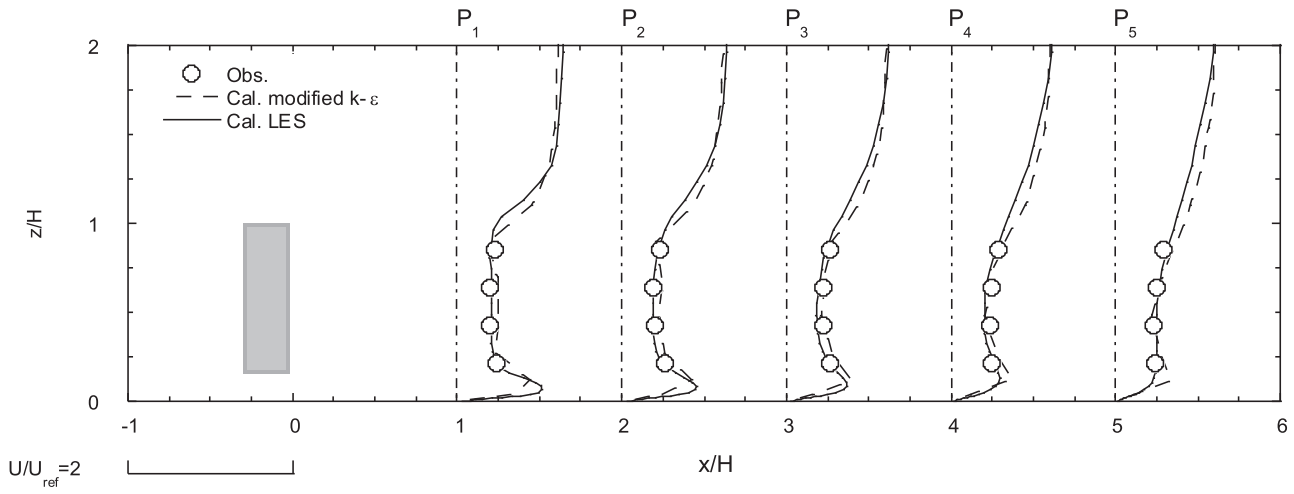

(a) Normalized mean wind speed

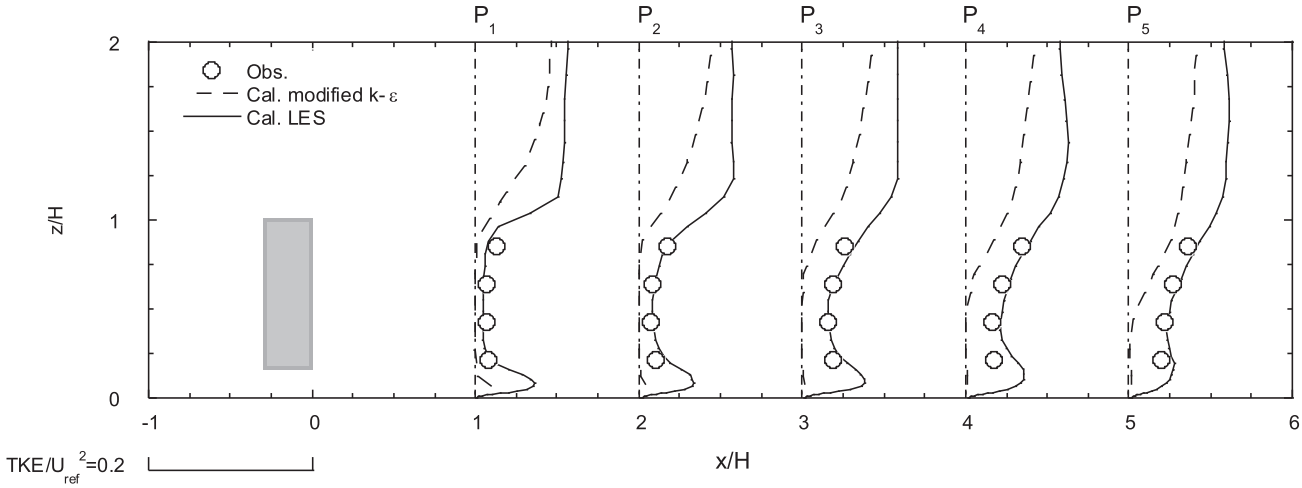

(b) Normalized turbulent kinetic energy

Fig. 5. Predicted and measured profiles of mean wind speed and turbulent kinetic energy behind the row of trees. The rectangular in gray marks the canopy region occupied by trees.

$\lambda_2 = -2000$. To represent the vortices in the wake region clearly, the central part of the computational domain with 50 m in lateral direction is used. In the bird's eye view as shown in Fig. 8, the roller structures of vortex generated at the top and bottom of trees are almost two dimensional and merge at the downward locations.

Fig. 9 shows the results of ΔS at the selected locations in the streamwise direction at the height of $z/H = 0.643$. In the upstream region of the row of trees, the values of $\Delta S(uw)$ and $\Delta S(uv)$ are close to zero, which indicate that the organized motions in this region are weak, as shown in Fig. 8. However, in the wake region, the organized motions in the vertical direction become strong. It is also worth to note that the value of $\Delta S(uw)$ is positive, indicating that the sweep motion is stronger than the ejection motion, thus the downward motion is dominant and the main source of turbulence in the wake region is transported from the top of tress. On the other hand, the values of $\Delta S(uv)$ are small not only in the upstream region but also in the wake, which express the organized motions in the lateral direction are weak because the flow field is almost two dimensional. Considering $k-\varepsilon$ models are designed and calibrated for fully developed flow fields, this analysis shows a possible reason why the modified $k-\varepsilon$ model is incapable of reproducing the turbulence in the wake region.

The modified $k-\varepsilon$ model underestimates the turbulent kinetic energy in the wake region due to lack of the organized motions generated at the top and bottom of trees. The LES model improves the accuracy of prediction because all large vortices generated are directly resolved in the simulation.

3.2. *Turbulent flow field around an isolated building*

The experimental data around an isolated building from the wind tunnel test as shown in Fig. 10 carried out by Meng and Hibi (1998) was selected to evaluate the performance of turbulence models (Mochida et al., 2002). The experiment was conducted in a return wind tunnel with a test section of 1.1 m wide, 0.9 m high and 7 m long. The dimensions of the isolated building in longitudinal, lateral and vertical directions are 0.08 m, 0.08 m and 0.16 m, respectively. The neutrally stratified atmospheric boundary layer was generated by five spires and a fence of height 0.6 m and 0.1 m respectively, which are designed following the method proposed by Irwin (1979). Three types of cubic blocks with heights of 0.06 m, 0.02 m and 0.01 m, are used downstream of the fence to adjust the lower part of boundary layer. Reynolds number based on the width of the isolated building and the mean velocity of the incident flow at the

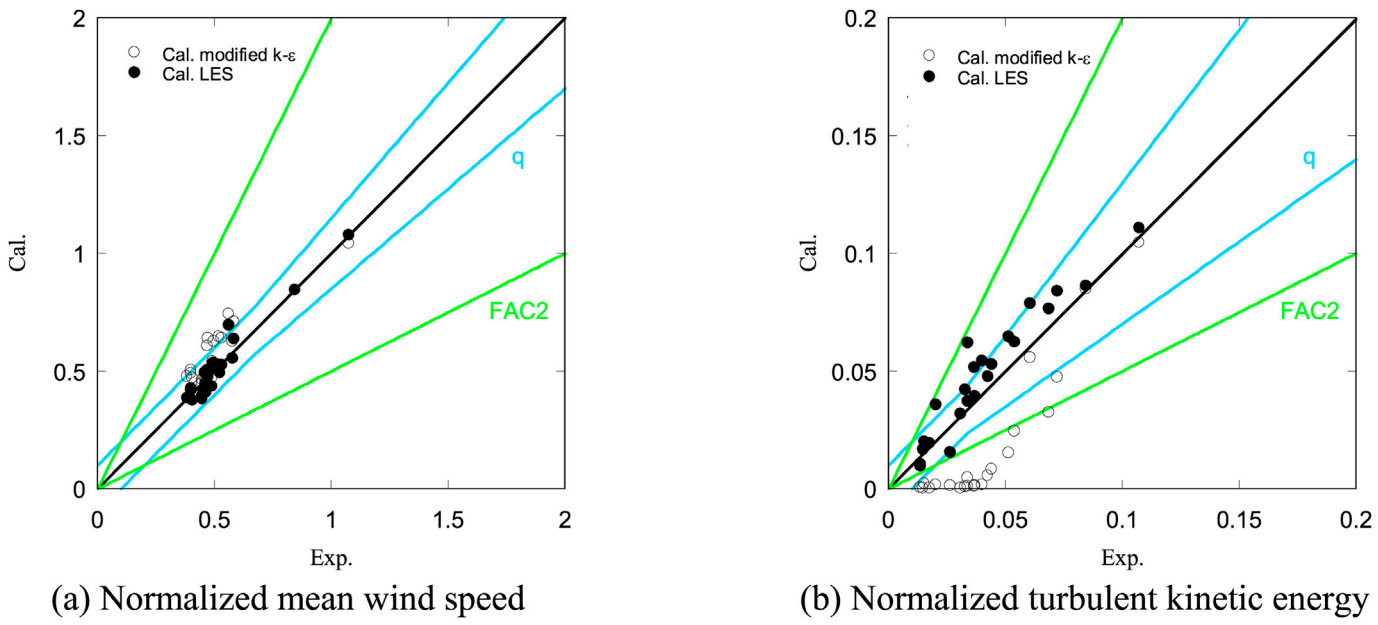

Fig. 6. Scatter plots of numerical results against experimental data for the case of the row of trees. The lines in blue and green mark the boundaries defined by ***q*** and FAC2, respectively. (For interpretation of the references to colour in this figure legend, the reader is referred to the Web version of this article.)

Table 4
Validation metrics for the case of the row of trees.

Turbulence Model	U/U_{ref}		$TKE/U_{ref}{}^2$	
	q	FAC2	q	FAC2
Modified $k-\varepsilon$	0.70	1.00	0.13	0.17
LES	0.96	1.00	0.78	1.00

building height is 2.4×10^4.

The computational domain for the simulation with LES model as shown in Fig. 11 is set as the same as the wind tunnel test. Spires and a fence with the same size as those in the wind tunnel test are used to generate turbulent inflow. Effects of cubic blocks are simulated by using the canopy model. According to the size of each type of cubic blocks, representative length scales are selected as $l_0 = 0.06$ m, $l_0 = 0.02$ m and $l_0 = 0.01$ m respectively. The same packing density $\gamma_0 = 6.25\%$ and equivalent drag coefficient $C_f = 1.981$ are adopted. In the simulation with the modified $k-\varepsilon$ model, the dimensions in lateral and vertical directions are the same as those in the simulation with LES model. One typical problem in the simulation with the modified $k-\varepsilon$ model, as discussed by Blocken et al. (2007), is unintended longitudinal gradients of the mean wind speed through the computational domain. A short longitudinal length for the simulation with the modified $k-\varepsilon$ model is set as 21 h = 1.68 m. The size of computational domain L_x, L_y and L_z are1.68 m, 1.1 m and 0.9 m, respectively.

A structural grid system is used in simulation with the modified $k-\varepsilon$ model, and $100 \times 86 \times 52$ grid nodes is used in the streamwise, lateral and vertical directions, respectively. A non-uniform grid is adopted in each direction. The minimum grid resolutions in the horizontal and vertical directions are 0.008 m and 0.004 m, respectively. In LES simulation, a structural grid system is also used in the region around the isolated building, while an unstructured grid is used around the spires and the fence. In the region around the isolated building, the minimum grid resolutions in the horizontal and vertical directions are 0.004 m and 0.002 m, respectively. Grid dependency is checked for both simulations by using twice finer grids around the building. The same profiles are obtained, indicating the present grid is fine enough.

The boundary conditions summarized in Table 2 are used for the simulations with the modified $k-\varepsilon$ model and LES model. In the simulation with the modified $k-\varepsilon$ model, $z_0 = 1.8 \times 10^{-5}m$ is used for the ground surface. In the simulation with LES model, an uniform wind speed of 6.75 m/s is set at the inlet boundary. The isolated building is treated as a canopy region. The canopy parameters, C_f, γ_0 and l_0, are calculated following Enoki and Ishihara (2012). To avoid dividing by zero, the packing density inside the isolated building is set as $\gamma_0 =$ 99.9999%.

The predicted and measured profiles of mean wind speed and turbulent kinetic energy at the location P_0 are shown in Fig. 12. The turbulent wind flow at the front of the isolated building is favourably reproduced well by the modified $k-\varepsilon$ model and LES model.

The normalized mean wind speed and turbulence kinetic energy profiles over isolated building in the vertical cross section at y/H = 0 and the horizontal cross section at z/H = 0.625 are shown in Fig. 13 and Fig. 14. Here, U_{ref} is the mean wind speed at x/H = 0 and z/H = 4 in the absence of isolated building. In case of the modified $k-\varepsilon$ model, the speed up phenomenon at the roof height and the mean wind speed in the wake region of the isolated building are slightly underestimated, while the predicted turbulent kinetic energy are overestimated at the region close to the isolated building and slightly underestimated in the wake region. The discrepancy in the wake region may be accounted by inability of the modified $k-\varepsilon$ model to simulate the organized motion, such as vortex shedding. This is discussed later. On the other hand, in case of the LES model, both mean wind speed and turbulent kinetic energy are well predicted.

Scatter plots of numerical simulation results against experimental data are shown in Fig. 15, and the validation metrics are summarized in Table 5. All validation metrics give the same conclusion that the LES model provides better accuracy than the modified $k-\varepsilon$ model with the generalized canopy model.

The contour of predicted mean wind speed and turbulent kinetic energy in the vertical and horizontal cross sections from the simulation with LES model are shown in Fig. 16 and Fig. 17. The streamlines are also plotted to describe reverse flow at the roof, side and wake of the isolated building. The contour of turbulent kinetic energy represents the turbulence generated in the region close to the building and transported to the wake region.

The iso-surface of λ_2 is used to represents the vortices generated by the isolated building as shown in the bird's eye view in Fig. 18. The block in light blue marks the canopy region occupied by the isolated building

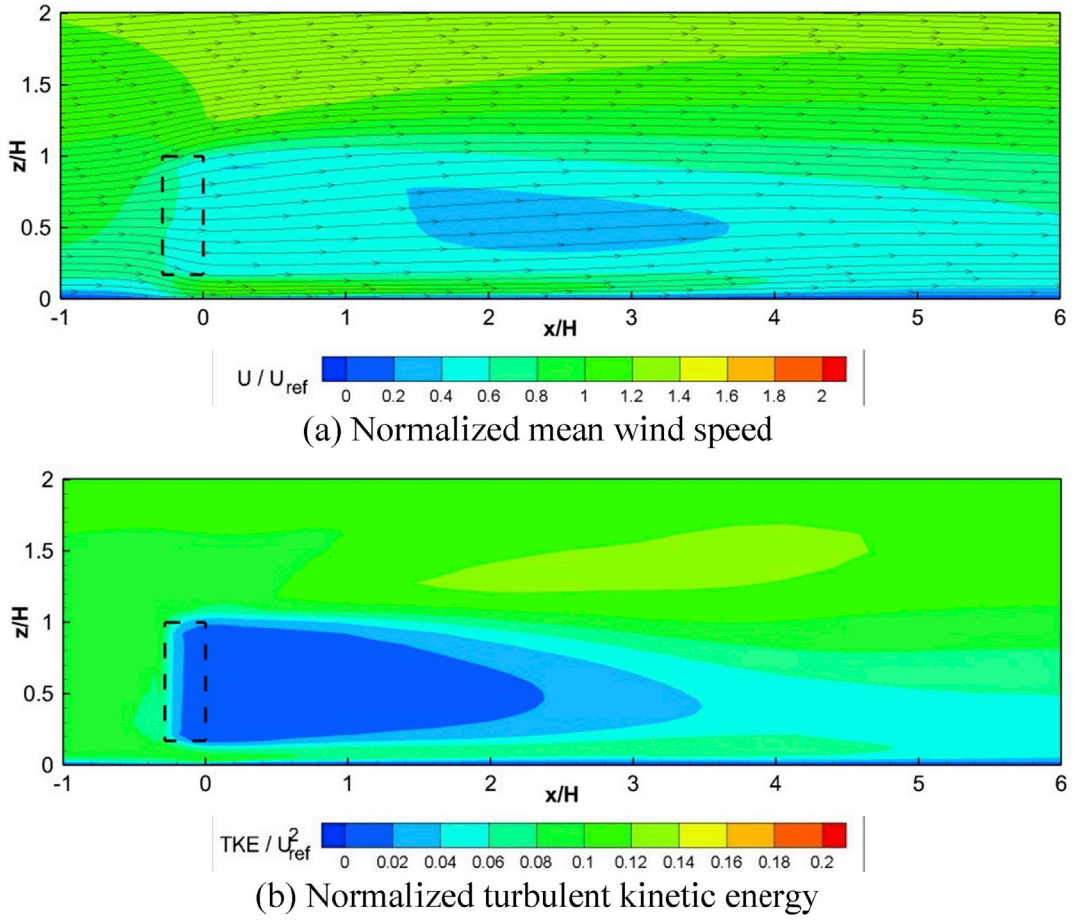

Fig. 7. Statistical Flow fields over the row of trees in cross section of y/H = 0.

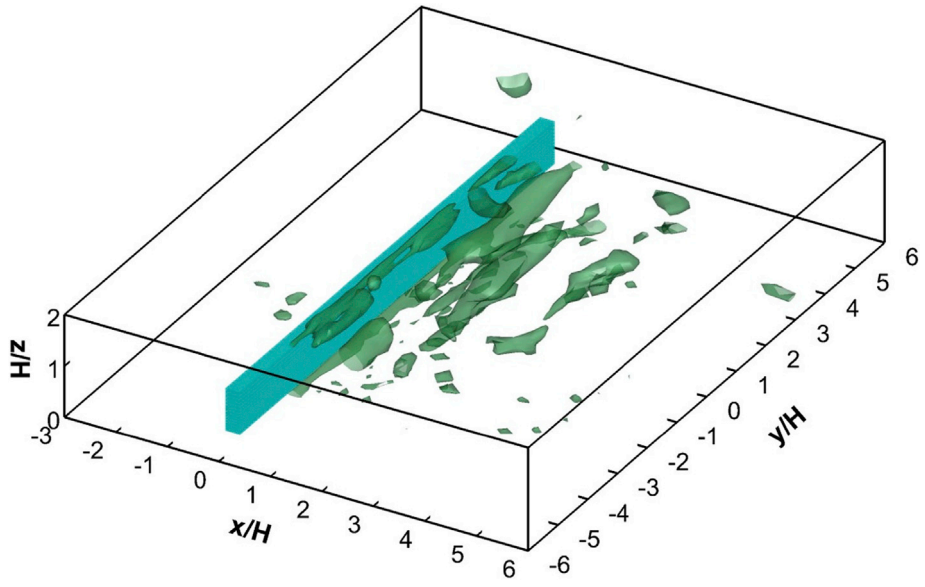

Fig. 8. Bird's eye view of instantaneous vortices with $\lambda_2 = -2000$ around the row of trees.

and the iso-surface in green indicates vortex cores with the value of $\lambda_2 = -10000$. It is clear that the large vortices generated by the edge of the isolated building move into the near wake region and then break into smaller pieces in the downstream region. The vortices shed from the edge of the isolated building are composed of a group of vortices and generate the high turbulence in this region.

Fig. 19 shows ΔS(uw) and ΔS(uv) at the selected locations and height of z/H = 0.5. It is found that both ΔS(uw) and ΔS(uv) shown in Fig. 19 (a) are small in the upstream of isolated building since organized motions are weak in the front area of the isolated building as shown in Fig. 18. In

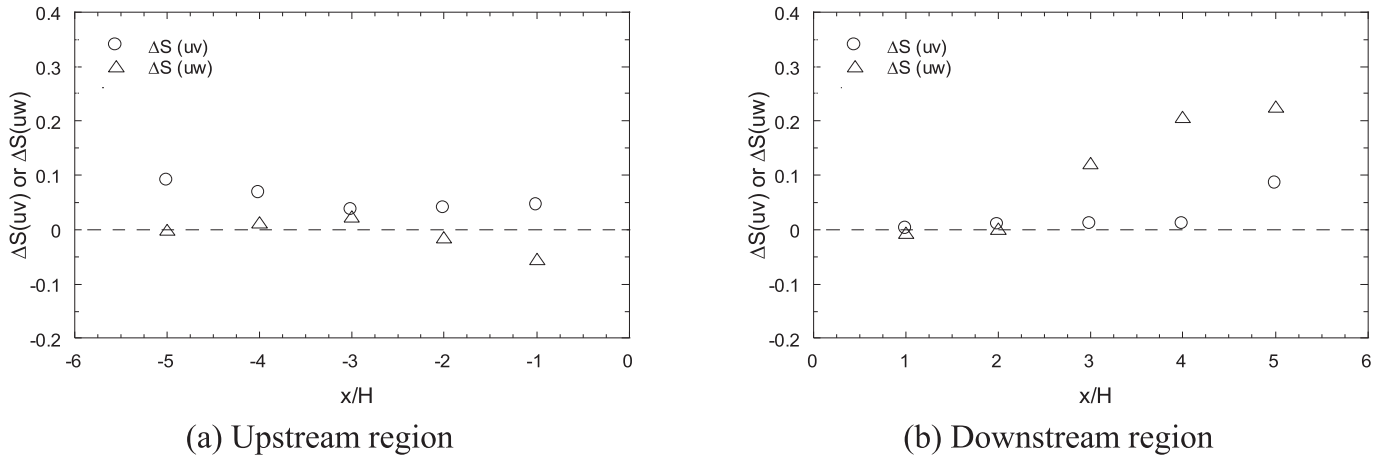

Fig. 9. Variation of **ΔS** with the downstream distance at the height of z/H = 0.643 for the case of the row of trees.

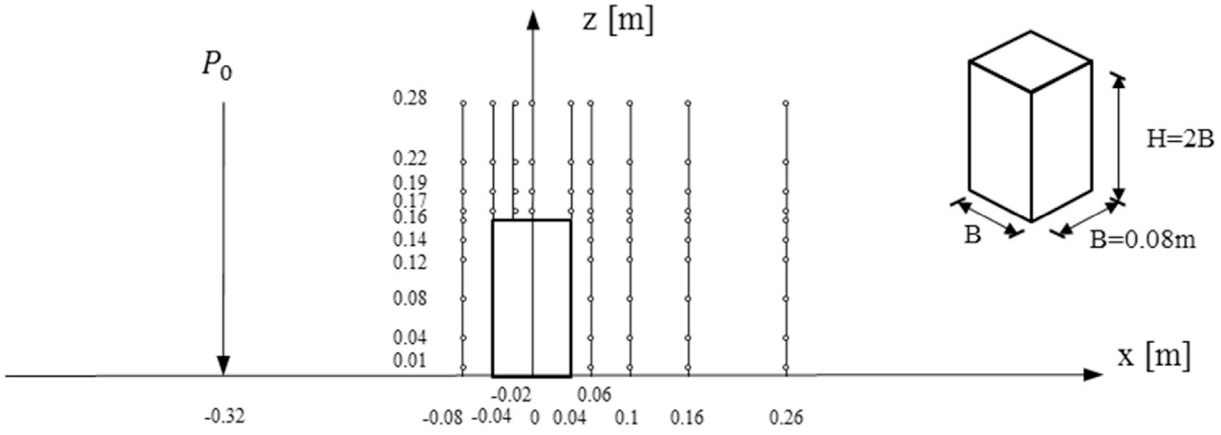

Fig. 10. Layout and measurement positions of an isolated building.

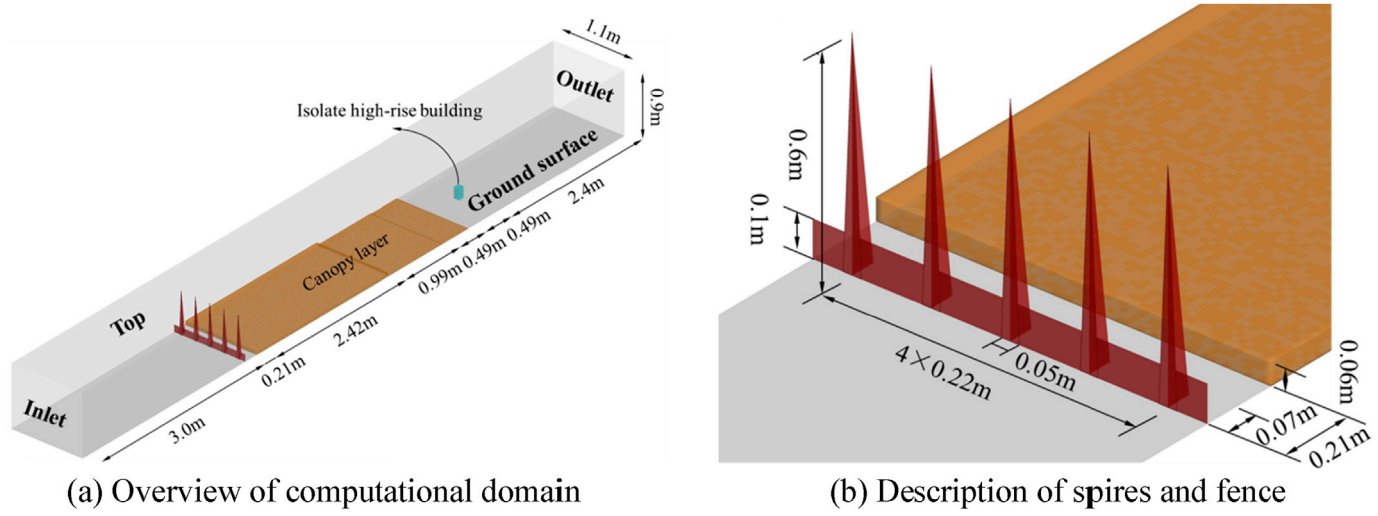

Fig. 11. Configuration of the numerical simulation of an isolated building with LES model.

the wake region, ΔS(uv) become strong and reaches the maximum at the location of x/H = 1. These strong horizontal organized motions correspond to the vortex shedding from the side edges of the isolated building as discussed above. With increasing of the downstream distance the value of ΔS(uv) decreases, indicating the decrease in intensity of horizontal organized motion. On the other hand, ΔS(uw) are small not only in the upstream region but also in the wake region at the height of z/H = 0.5. Therefore, it is concluded that the turbulent kinetic energy at this height are mainly generated from the side edges of the isolated building.

As a conclusion, the modified $k-\varepsilon$ model slightly underestimates the turbulent kinetic energy in the wake region due to lack of the vortex shedding in the simulation, while the LES model improves the accuracy of prediction since all large vortices are directly resolved.

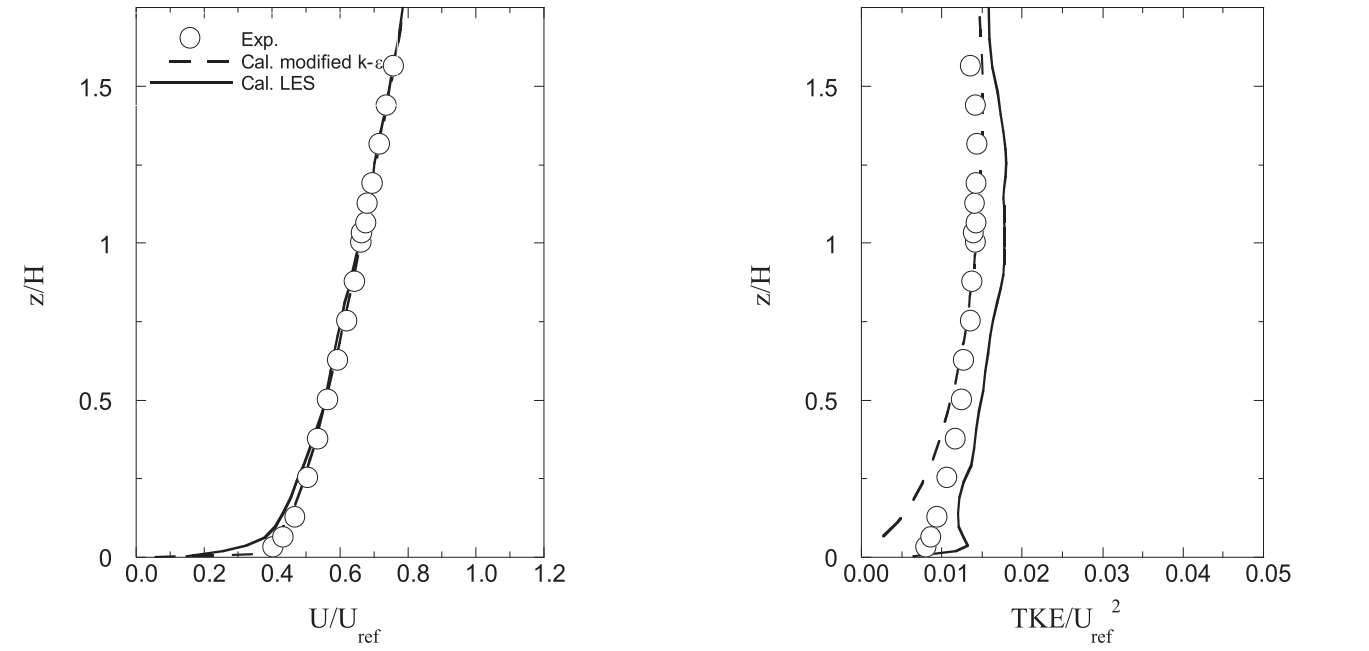

Fig. 12. Predicted and measured profiles of mean wind speed and turbulent kinetic energy at the location P0 for the case of the isolated building.

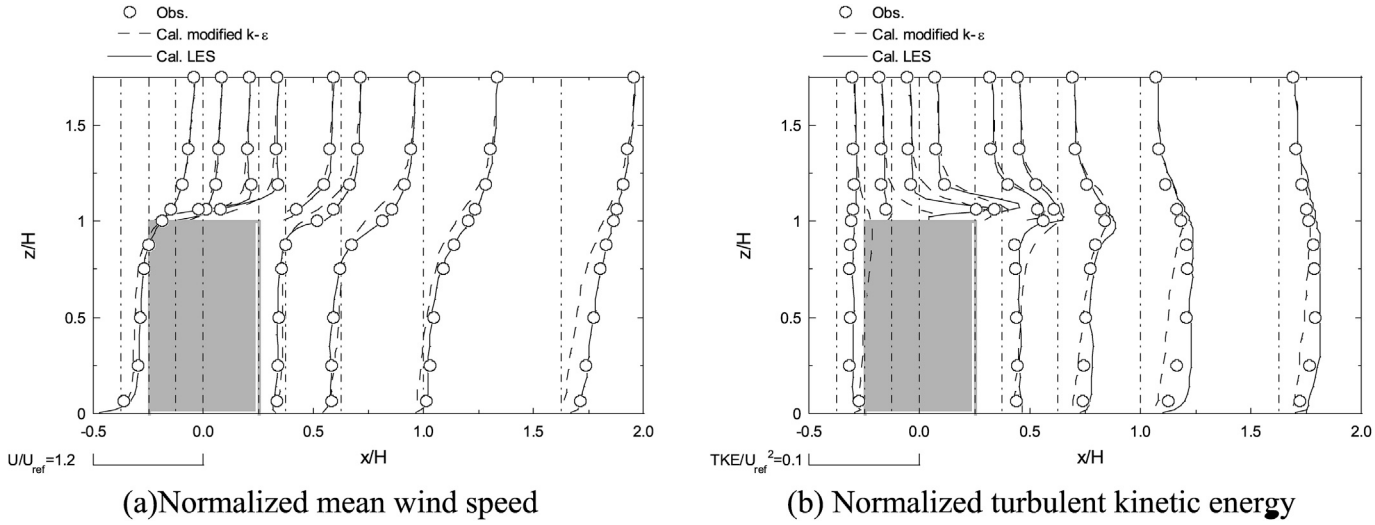

Fig. 13. Predicted and measured profiles of mean wind speed and turbulent kinetic energy around the isolated building in the vertical cross section at y/H = 0.

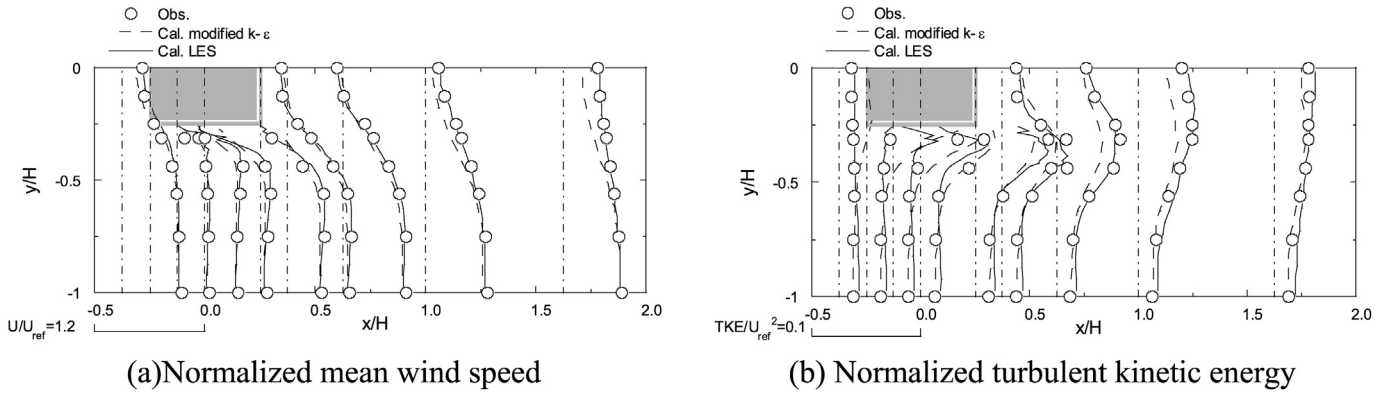

Fig. 14. Predicted and measured profiles of mean wind speed and turbulent kinetic energy around the isolated building in the horizontal cross section at z/H = 0.625.

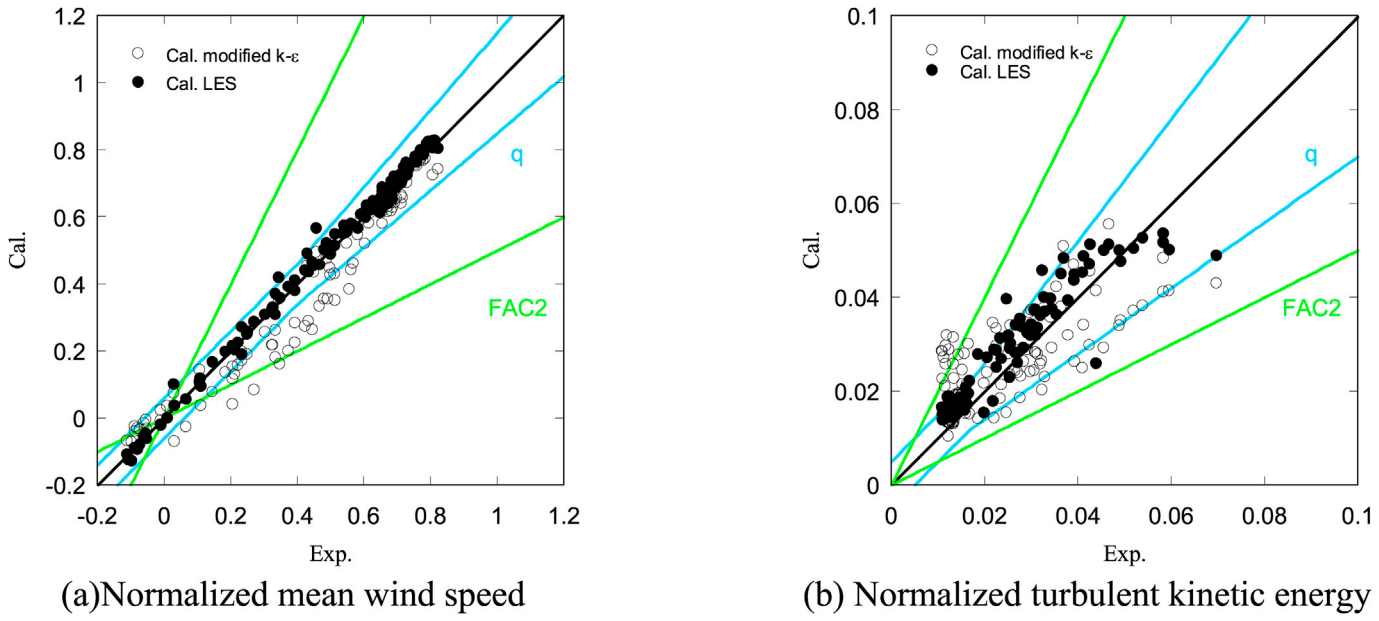

Fig. 15. Scatter plots of numerical simulation results against experimental data for the case of the isolated building. The lines in blue and green mark the boundaries defined by ***q*** and FAC2, respectively. (For interpretation of the references to colour in this figure legend, the reader is referred to the Web version of this article.)

Table 5
Validation metrics for the case of an isolated building.

Turbulence Model	U/U_{ref}		TKE/U_{ref}^2	
	q	FAC2	q	FAC2
Modified $k-\varepsilon$	0.74	0.89	0.70	0.92
LES	0.98	0.97	0.86	1.00

4. Conclusions

In this study, turbulent flow fields over two typical urban elements, a row of trees with low packing density and an isolated building with high packing density, are investigated by the modified $k-\varepsilon$ model and the LES model incorporated with a generalized canopy model. The following conclusions are obtained.

1) The applicability of the modified $k-\varepsilon$ model and LES model is evaluated by the validation metrics. Two turbulence models provide accurate mean wind speed and turbulent kinetic energy in the front areas of the row of trees and the isolated building. However, in the wake region, LES model shows better performance than the modified $k-\varepsilon$ model.
2) The turbulent flow fields predicted by LES model around the row of trees and the isolated building are visualized by vortex cores and examined by the quadrant analysis. It is found that the organized motions generated at the top and bottom of trees are dominant in the wake region of the row of trees, while the organized motions due to the vortex shedding from the building surface are dominant in the wake region of the isolated building. The mean wind speed and turbulent kinetic energy for two cases are well predicted by LES model.
3) The mean wind speed in the wake region of the row of trees is favourably predicted by the modified $k-\varepsilon$ model, but the turbulent kinetic energy is significantly underestimated due to the deficiency of the organized motions in the simulation with the modified $k-\varepsilon$ model. The mean wind speed and turbulent kinetic energy by the modified $k-\varepsilon$ model in the wake region of the isolated building are

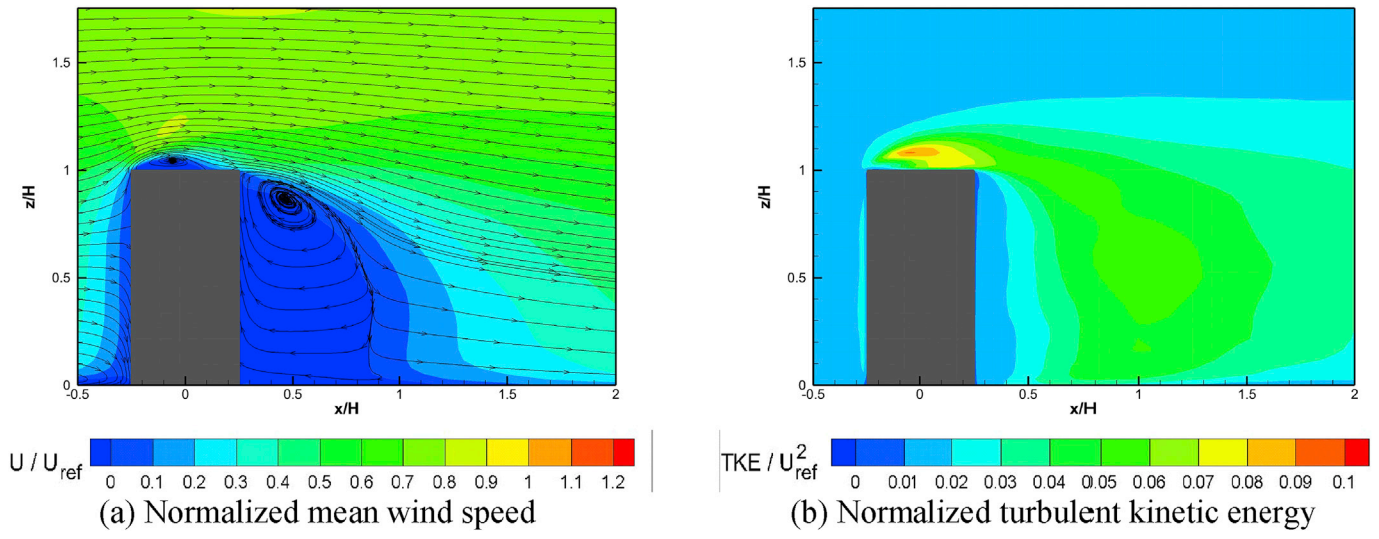

Fig. 16. Statistical flow fields around the isolated building in cross section of y/H = 0. The block in gray marks the canopy region occupied by the isolated building.

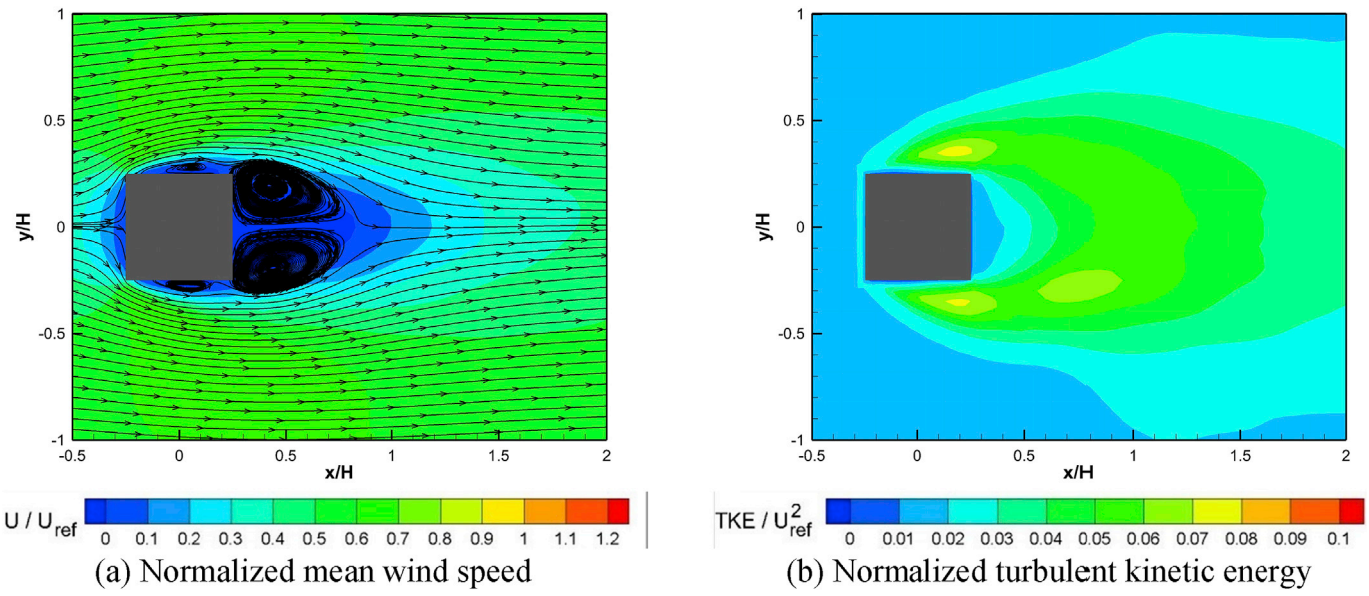

Fig. 17. Statistical flow fields around the isolated building in cross section z/H = 0.625. The block in gray marks the canopy region occupied by the isolated building.

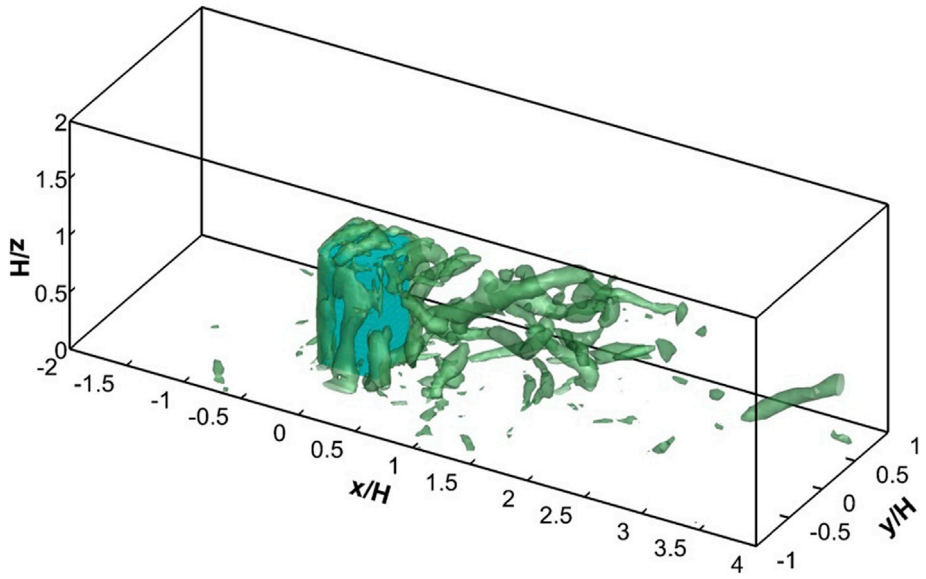

Fig. 18. Bird's eye view of instantaneous vortex with $\lambda_2 = -10000$ around the isolated building.

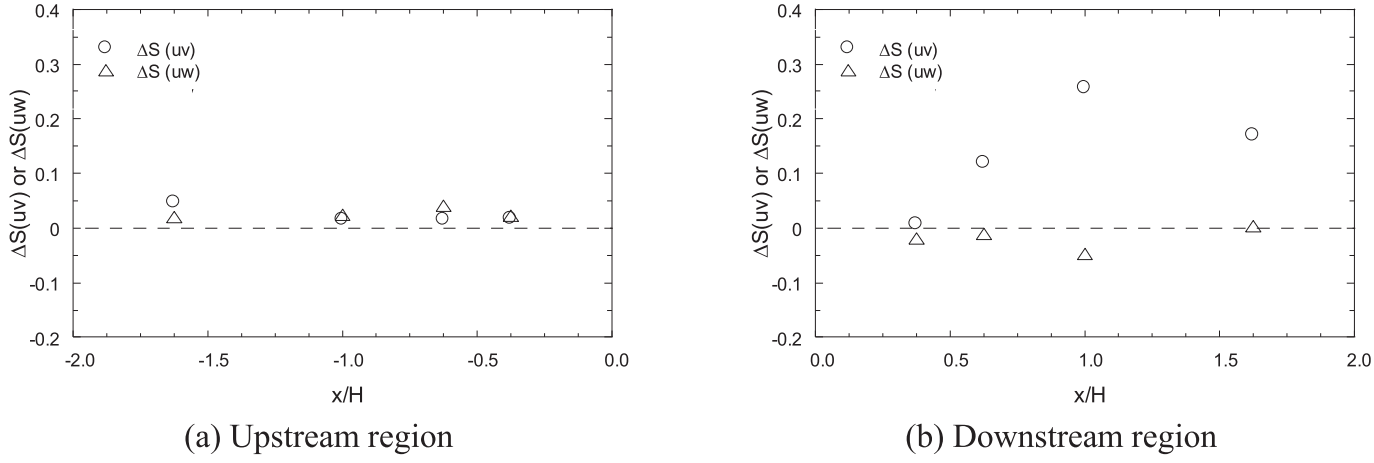

Fig. 19. Variation of ΔS with the downstream distance at the height of z/H = 0.5 for the case of the isolated building.

also slightly underestimated due to lack of the vortex shedding in the wake region.

References

Aumond, P., Masson, V., Lac, C., Gauvreau, B., Dupont, S., Berengier, M., 2013. Including the drag effects of canopies: real case large-eddy simulation studies. Boundary-Layer Meteorol. 146 (1), 65–80.

Bailey, B.N., Stoll, R., 2013. Turbulence in sparse, organized vegetative canopies: a large-eddy simulation study. Boundary-Layer Meteorol. 147 (3), 369–400.

Blocken, B., Stathopoulos, T., Carmeliet, J., 2007. CFD simulation of the atmospheric boundary layer: wall function problems. Atmos. Environ. 41 (2), 238–252.

Blocken, B., Janssen, W., van Hooff, T., 2012. CFD simulation for pedestrian wind comfort and wind safety in urban areas: general decision framework and case study for the Eindhoven University campus. Environ. Model. Software 30, 15–34.

Cheng, W.-C., Porté-Agel, F., 2015. Adjustment of turbulent boundary-layer flow to idealized urban surfaces: a large-eddy simulation study. Boundary-Layer Meteorol. 155 (2), 249–270.

Enoki, K., Ishihara, T., 2012. A generalized canopy model and its application to the prediction of urban wind climate. J. Jpn. Soci. Civ. Eng. Ser. A1 (Struct. Eng. Earthq. Eng) 68 (1), 28–47 (In Japanese).

Enoki, K., Ishihara, T., Yamaguchi, A., 2009. A generalized canopy model for the wind prediction in the forest and the urban area. In: Proc. Of EWEC 2009.

Gousseau, P., Blocken, B., Stathopoulos, T., Van Heijst, G., 2011. CFD simulation of near-field pollutant dispersion on a high-resolution grid: a case study by LES and RANS for a building group in downtown Montreal. Atmos. Environ. 45 (2), 428–438.

Gousseau, P., Blocken, B., Van Heijst, G., 2013. Quality assessment of large-eddy simulation of wind flow around a high-rise building: validation and solution verification. Comput. Fluids 79, 120–133.

Green, S., 1992. Modelling turbulent air flow in a stand of widely-spaced trees. Phoenics J 5 (3), 294–312.

IEC 61400-2, I., 2006. Wind Turbines–part 2: Design Requirements for Small Wind Turbines.

Irwin, H., 1979. Design and use of spires for natural wind simulation. National Research Council, Canada. LTR-LA-233.

Iwata, T., Kimura, A., Mochida, A., Yoshino, H., 2004. Optimization of tree canopy model for CFD prediction of wind environment at pedestran level. In: Proceedings of National Symposium on Wind Engineering (In Japanese).

Jeong, J., Hussain, F., 1995. On the identification of a vortex. J. Fluid Mech. 285, 69–94.

Kato, M., 1993. The modeling of turbulent flow around stationary and vibrating square cylinders. In: Ninth Symposium on Turbulent Shear Flows, 1993.

Kida, S., Miura, H., 1998. Identification and analysis of vortical structures. Eur. J. Mech. B Fluid 17 (4), 471–488.

Kurotani, Y., Kiyota, N., Kobayashi, S., 2001. Windbreak effect of tsuijimatsu in Izumo: Part 2. In: Proceedings of Architectural Institute of Japan, pp. 745–746.

Liu, J., Chen, J., Black, T., Novak, M., 1996. E-ε modelling of turbulent air flow downwind of a model forest edge. Boundary-Layer Meteorol. 77 (1), 21–44.

Lopes, A.S., Palma, J., Lopes, J.V., 2013. Improving a two-equation turbulence model for canopy flows using large-eddy simulation. Boundary-Layer Meteorol. 149 (2), 231–257.

Maruyama, T., 1993. Optimization of roughness parameters for staggered arrayed cubic blocks using experimental data. J. Wind Eng. Ind. Aerod. 46, 165–171.

Meng, Y., Hibi, K., 1998. Turbulent measurements of the flow field around a high-rise building. J. Wind Eng. 1998 (76), 55–64 (In Japanese).

Mochida, A., Tominaga, Y., Murakami, S., Yoshie, R., Ishihara, T., Ooka, R., 2002. Comparison of various k-ε models and DSM applied to flow around a high-rise building - report on AIJ cooperative project for CFD prediction of wind environment. Wind Struct. 5 (2–4), 227–244.

Mochida, A., Tabata, Y., Iwata, T., Yoshino, H., 2008. Examining tree canopy models for CFD prediction of wind environment at pedestrian level. J. Wind Eng. Ind. Aerod. 96 (10), 1667–1677.

Mueller, E., Mell, W., Simeoni, A., 2014. Large eddy simulation of forest canopy flow for wildland fire modeling. Can. J. For. Res. 44 (12), 1534–1544.

Oikawa, S., Meng, Y., 1995. Turbulence characteristics and organized motion in a suburban roughness sublayer. Boundary-Layer Meteorol. 74 (3), 289–312.

Oka, S., Ishihara, T., 2009. Numerical study of aerodynamic characteristics of a square prism in a uniform flow. J. Wind Eng. Ind. Aerod. 97 (11), 548–559.

Philips, D., Rossi, R., Iaccarino, G., 2013. Large-eddy simulation of passive scalar dispersion in an urban-like canopy. J. Fluid Mech. 723, 404–428.

Rodi, W., 1997. Comparison of LES and RANS calculations of the flow around bluff bodies. J. Wind Eng. Ind. Aerod. 69, 55–75.

Salim, M.H., Schlünzen, K.H., Grawe, D., 2015. Including trees in the numerical simulations of the wind flow in urban areas: should we care? J. Wind Eng. Ind. Aerod. 144, 84–95.

Schatzmann, M., Olesen, H., Franke, J., 2010. COST 732 Model Evaluation Case Studies: Approach and Results, 121 pp. COST Office Brussels, ISBN, p. 3–00.

Suzuki, J., Yoshida, S., Ooka, R., Kurotani, Y., 2002. Study on windbreak effect of Tsujimatsu in Izumo using CFD analysis. In: Summaries of Technical Papers of Annul Meeting Architectural Institute of Japan 2002 (In Japanese).

Tominaga, Y., Mochida, A., Murakami, S., Sawaki, S., 2008. Comparison of various revised k–ε models and LES applied to flow around a high-rise building model with 1: 1: 2 shape placed within the surface boundary layer. J. Wind Eng. Ind. Aerod. 96 (4), 389–411.

Wilson, J., 1988. A second-order closure model for flow through vegetation. Boundary-Layer Meteorol. 42 (4), 371–392.

Xie, Z., Castro, I.P., 2006. LES and RANS for turbulent flow over arrays of wall-mounted obstacles. Flow, Turbul. Combust. 76 (3), 291–312.

Yang, B., Raupach, M.R., Shaw, R.H., Paw U, K.T., Morse, A.P., 2006. Large-eddy simulation of turbulent flow across a forest edge. Part I: flow statistics. Boundary-Layer Meteorol. 120 (3), 377–412.

Yoshie, R., Mochida, A., Tominaga, Y., Kataoka, H., Harimoto, K., Nozu, T., Shirasawa, T., 2007. Cooperative project for CFD prediction of pedestrian wind environment in the Architectural Institute of Japan. J. Wind Eng. Ind. Aerod. 95 (9), 1551–1578.

Yoshie, R., Jiang, G., Shirasawa, T., Chung, J., 2011. CFD simulations of gas dispersion around high-rise building in non-isothermal boundary layer. J. Wind Eng. Ind. Aerod. 99 (4), 279–288.